Modeling of NQS Effects in Carbon Nanotube Transistors

Martin Claus, Sven Mothes, Michael Schröter
Chair for Electron Devices and Integrated Circuits, Technische Universität Dresden, Dresden, Germany
Phone: +49 351 463-33053, Fax: +49 351 463-37260, email: martin.claus@tu-dresden.de

Abstract

Time-dependent quantum simulations are used to rigorously identify non-quasi-static (NQS) effects in Carbon nanotube transistors. A complete physics-based small signal equivalent circuit is derived which captures important NQS effects for circuit design and simulation. This model agrees well with high-frequency measurements. Additionally, the impact of Schottky barriers on the kinetic inductance and the charging resistances is discussed and the role of the contact resistances is investigated.

Introduction

Carbon nanotube field effect transistors (CNTFETs) are promising candidates for high-frequency (HF) analog applications due to their high intrinsic transconductance and very low intrinsic capacitances per tube. Regardless of all difficulties [1] in measuring the HF behavior of fabricated CNTFETs, measured HF figures of merit such as the transit frequency f_T indicate that they are far away from their expected intrinsic values.

Albeit the present challenges [2], [3], the intrinsic HF potential is still under investigation. Time-dependent transport simulations either based on the Boltzmann equation [4] or Schrödinger equation [5] are considered to account for non-quasi-static (NQS) effects describing the delay of the charge carriers in response to fast signal variations at the device terminals.

Current pre-production technologies show tube lengths of around $500\,n$m. For such long devices, $f_\mathrm{T,int}$ is about 1 to $10\,G$Hz. Therefore, practical HF applications demand CNTFETs to operate near peak f_T. With carefully optimized layout and dense parallel tubes, the parasitic capacitances per tube can be reduced to approach $f_\mathrm{T,int}$.

In the present paper we use time-dependent self-consistent quantum simulations to derive a physics-based small-signal equivalent circuit which captures important NQS effects and which is valid for all bias points and frequencies needed for circuit design and simulation. Finally, we apply our model to measurements and discuss the impact of NQS effects.

Quantum model

To accurately model the transmission properties of a CNTFET in the ballistic limit, we solve self-consistently the Poisson equation with the time-dependent one-dimensional effective-mass Schrödinger equation [5], [6], [7]. We consider a Crank-Nicholson finite difference scheme for a stable time-dependent numerical solution. To minimize numerical reflections at the boundaries, we implemented discrete transparent boundary conditions [8]. Furthermore, properly chosen boundary conditions model the impact of contact details like Schottky barriers and hybridization. Realistic 3D planar contact geometries allows to study electrostatic coupling effects.

In the first part of this work we simulated a $50\,n$m long CNTFET. All parameters are adapted to the measurements published in [9]. A good agreement of DC simulation results to the measured data is achieved. The contact geometry induces parasitics, e. g. metal-metal capacitances and feed-line resistances. However, for a physics-based well-defined separation of the intrinsic transistor from parasitic effects, these contact parasitics are ignored within our simulations.

The method proposed in [10] is used to extract the frequency-dependent admittance parameters Y^ac of a common source CNTFET by transient excitation of the device terminals followed by Fourier decomposition.

NQS modeling

For a systematic identification of the various NQS effects we compare the simulated admittance parameters Y^ac to two-port quasi-static and non-quasi-static admittance parameters Y^qs and Y^nqs, respectively. Both, Y^qs and Y^nqs are based on the equivalent circuit described below.

The non-quasi-static equivalent circuit shown in Fig. 1 is based on [11]. In comparison to the quasi-static equivalent circuit [12], the branch capacitances C_gs and C_gd are replaced with $RLC-$series combinations and the output impedance consists of a resistance in series with an inductance. The frequency dependence of the transconductance is given by

$$g_\mathrm{m} = \frac{g_\mathrm{m0}}{1 + jw\tau_1 - (w\tau_2)^2} \tag{1}$$

where the time constants $\tau_1 = C_\mathrm{m}/g_\mathrm{m0}$ and $\tau_2 = \sqrt{L_\mathrm{m}C_m}$ depend on the low-frequency transconductance g_m0, C_m and the channel inductance L_m. In the QS model, the frequency dependence of the transconductance equals

$$g_\mathrm{m} = g_\mathrm{m0} - j\omega C_\mathrm{m} \tag{2}$$

where $C_\mathrm{m} = C_\mathrm{gd} - C_\mathrm{dg}$ models the non-reciprocity of the gate-drain capacitance. Fig. 2 – 4 show admittance parameters based on quantum transient simulations ($V_\mathrm{gs} = -0.5\,$V) in comparison to the admittance parameters based on the quasi-static and non-quasi-static equivalent circuits. The values for the circuit elements are fitted to Y^ac to give the best agreement (see Tab. I).

978-1-4244-7700-5/10/$26.00 ©2010 IEEE

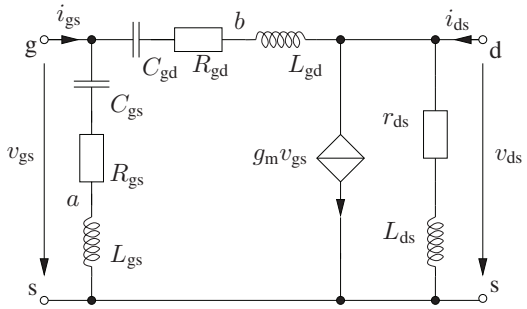

Fig. 1. Complete non-quasi-static equivalent circuit for the intrinsic transistor valid for frequencies up to $10\,THz$. The charging resistances R_{gs} and R_{gd}, the inductances and the complex valued transconductance g_m model the NQS effects.

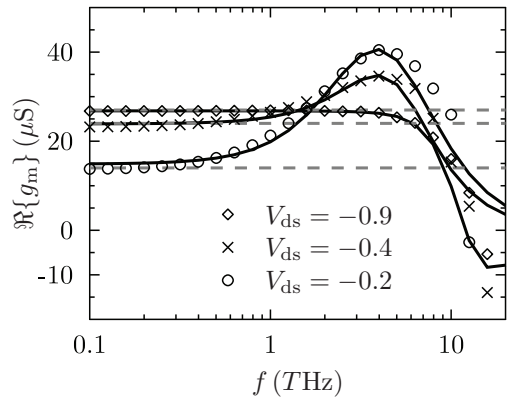

Fig. 2. Frequency characteristic of the real part of the transconductance g_m based on Y^{ac} (symbols) compared to the NQS model (solid line) and the QS model (dashed line).

Comparing the data shown in the figures, it can be observed that

(*i*) the real part of the transconductance $g_m = Y_{21}^{ac} - Y_{12}^{ac}$ shows peaking and a fall-off with frequency (cf. Fig. 2),

(*ii*) the input admittance Y_{11}^{ac} is not entirely capacitive (cf. Fig. 3) at high frequencies,

(*iii*) the output admittance Y_{22}^{ac} shows inductive behavior at high frequencies beyond $600\,GHz$ (cf. Fig. 4),

(*iv*) the imaginary part of Y_{11}^{ac} and Y_{12}^{ac} shows inductive behavior for highest frequencies (cf. Fig. 5).

It is interesting to note that phenomena (*i*) – (*iii*) - albeit calculated with a ballistic quantum model - are identical to the phenomena previously reported for MOS transistors [13].

Particularly, the inductive behavior of Y_{22}^{ac} was previously predicted for CNTFETs in [14], [15] and has been known for MOS transistors [12]. Even if the three groups use different transport models for their explanations, they describe eventually the inertia of the charge carriers in the case of fast varying potentials. For CNTFETs this effect was attributed to the so called *kinetic inductance L*. At moderate frequencies, the output current i_{ds} shows a delay in response to voltage changes at the output terminal. This

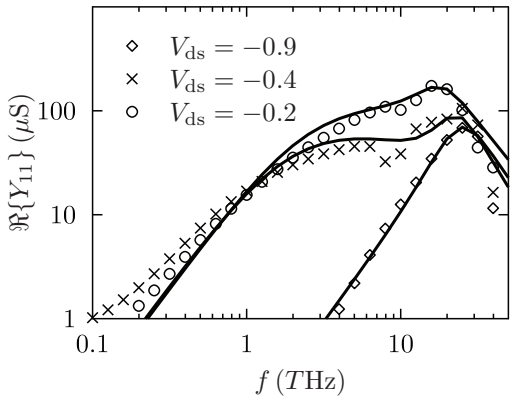

Fig. 3. Real part of the input impedance Y_{11}^{ac} (symbols) compared to the NQS model (solid line). The QS values equal zero and are not shown here.

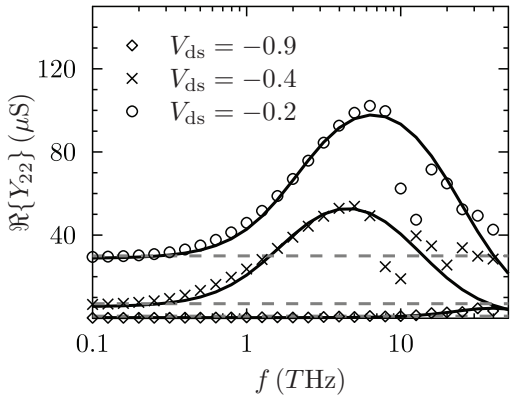

Fig. 4. Real part of the output impedance Y_{22}^{ac} (symbols) compared to the NQS model (solid line) and the QS model (dashed line). The non-continues symbols at $10\,THz$ are numerical artifacts.

delay is modeled with the kinetic inductance L_{ds} in series with the output resistance r_{ds} in the NQS equivalent circuit. At highest frequencies, kinetic inductances L_{gs} and L_{gd} should also be considered in branch a and b of the NQS equivalent circuit to model the delay of the gate current in response to voltage changes at the input and output terminal (cf. observation (*iv*)). The extracted values for L in Tab. I are in the range of theoretical predictions [14]. Since we simulate an intrinsic CNTFET without feed lines, the inductive behavior can not be attributed to feed line inductances. Additionally, $\tau_2 = \sqrt{L_m C_m}$ in the frequency characteristic of the transconductance g_m is needed to capture the resonance in the real part of g_m.

The charging resistances R_{gs} and R_{gd} in branch a and b of the NQS equivalent circuit model the finite charging time of the gate capacitances C_{gs} and C_{gd} leading to non-vanishing real parts of Y_{11}^{ac} and Y_{12}^{ac} and a phase shift approaching zero at high frequencies. For single-tube devices the charging resistances are fairly high ($\approx 10 - 100\,k\Omega$) and are related to the shape of the gate-source Schottky

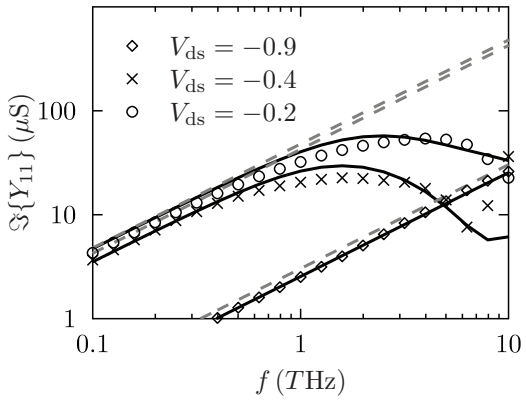

Fig. 5. Imaginary part of the input impedance Y_{11}^{ac} (symbols) compared to the NQS model (solid line) and the QS model (dashed line).

element	-0.2 V	-0.4 V	-0.9 V	meas.
C_{gs}	0.8 aF	0.42 aF	0.37 aF	5 aF/tube
R_{gs}	10 $k\Omega$	14 $k\Omega$	15 $k\Omega$	90 $k\Omega$/tube
L_{gs}	97 pH	110 pH	105 pH	–
C_{gd}	6.7 aF	5.2 aF	0.03 aF	2 aF/tube
R_{gd}	11 $k\Omega$	20 $k\Omega$	20 $k\Omega$	130 $k\Omega$/tube
L_{gd}	64 pH	210 pH	500 pH	–
r_{ds}	35 $k\Omega$	185 $k\Omega$	334 $k\Omega$	100$k\,\Omega$/tube
L_{ds}	2 nH	12 nH	80 nH	340 nH/tube
g_{m0}	15 μS	24 μS	27 μS	2.2 μS/tube
C_m	1 aF	1.1 aF	0.4 aF	20 fF/tube
L_m	380 pH	350 pH	410 pH	0.9 nH/tube
$f_{T,intr}$	340 GHz	640 GHz	10 THz	3.4 GHz

TABLE I. Extracted equivalent circuit elements. The first three columns contain the elements for the single-tube simulation study for $V_{ds} = -0.2, -0.4, -0.9$ V, respectively, while the last column contains averaged values for *semiconducting* tubes extracted from measurements. Note that the measured tubes are 10 times longer.

barrier. The thinner the Schottky barrier, the shorter the time the carriers need to transverse the barriers and, hence, the shorter the charging time.

Our simulation data indicate that all effects described above are well captured by the NQS equivalent circuit while the QS equivalent circuit gives only good results for frequencies below the intrinsic transit frequencies listed in Tab. I.

Parasitics

The impact of the parasitics on the HF behavior strongly depends on the contact geometry and the layout. For practical analog applications multi-finger and multi-tube transistors are needed to achieve sufficient output power [16]. An equivalent circuit including the metal-metal capacitances (C_{pgs}, C_{pgd}, C_{pds}) between the source, drain and gate fingers, the finger resistances R_{pg}, R_{ps}, R_{pd} and the finger inductances L_{pg}, L_{ps}, L_{pd} typical for multi-tube and multi-finger transistors is shown in Fig. 6.

In addition, "contact resistances" (R_{cs}, R_{cd}) need to be included. However, to our best knowledge, for ballistic and quasi-ballistic devices, the term "contact resistance" is still fuzzy. From measurement point of view it is unclear how to differ between ballistic transport effects within the tube from bias-independent effects induced by the contact physics. If measurements are compared to a CNTFET model where e. g. Schottky barriers are inlcuded, the contact resistance can not be attributed to them. Other effects like weak or strong metal-CNT hybridization can contribute but also change transport phenomena within the tube. Hence, due to the strong uncertainty how to extract unambiguously this resistance we will drop them for our studies in this paper. Nonetheless, we will see that our measurements are well described qualitatively without considering contact resistances[1]. We currently assume that the fairly high extracted *bias-dependent* charging resistances R_{gs} and R_{gd}, the high output resistance r_{ds} as well as the low transconductance g_{m0} shadow the impact of the (by definition) *bias-independent* contact resistances R_{cs} and R_{cd}.

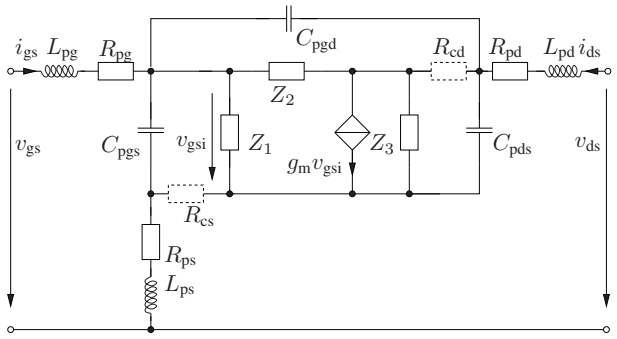

Fig. 6. Equivalent circuit including the parasitics typical for a multi-tube and multi-finger transistor. The $Z-$parameters are defined by the NQS equivalent circuit. The impact of the parasitics induced by the substrate are ignored for the frequency range measured.

Measurements

Since HF measurements of single-tube and single-finger transistors are very difficult, multi-tube devices are typically used to study the HF behavior.

Fig. 7 and 8 show de-embedded admittance parameters Y^{deemb} at $V_{ds} = -1$ V and $V_{gs} = -1.5$ V of a measured multi-tube, multi-finger top-gated CNTFET with approximately 2000 semiconducting and 500 metallic 500 nm long tubes in parallel. The gate is 200 nm long and centered within the channel. For de-embedding the intrinsic behavior an open structure is used that is identical to the transistor structure without tubes [13]. Albeit this technique does not cancel the effects of the series resistances R_{pg}, R_{pd} and R_{ps} as well as inductive components, detailed calculations show the series resistances and the interconnect inductances to be negligible for the given layout and frequencies of interest.

A comparison of Y^{deemb} with simulation results of the QS and NQS model shows that deviations from the QS model

[1]More detailed studies reveal that the contact resistance seems to be at maximum 5 to 10 $k\Omega$/tube for the measured device.

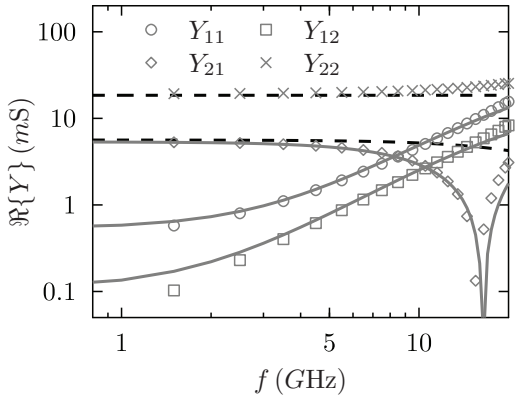

Fig. 7. Real parts of the measured admittance parameters (symbols) compared to the NQS model (solid lines) and QS model (dashed line). Due to a leaky gate oxide, a resistance of $R_a = 2\,k\Omega$ and $R_b = 10\,k\Omega$ are added in parallel to branch a and b of the NQS model.

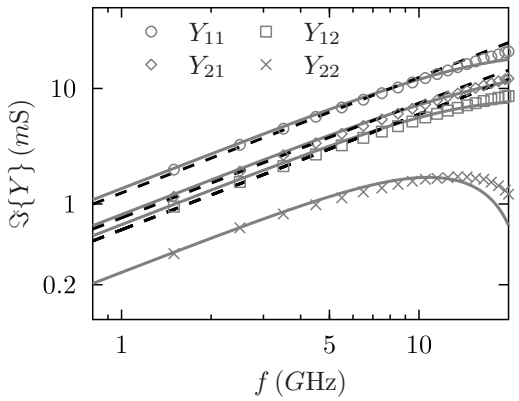

Fig. 8. Imaginary parts of the measured admittance parameters (symbols) compared to the NQS model (solid lines) and QS model (dashed line).

are visible at frequencies beyond the intrinsic transit frequency of $f_{\mathrm{T,int}} = 3.4\,G\mathrm{Hz}$. The de-embedded parameters are used to extract the average value of the equivalent circuit elements for *one* semiconducting tubes (see Tab. I). We simply model the small-signal behavior of metallic tubes by their quantum capacitance of around $400\,a\mathrm{F}/\mu\mathrm{m}$ per tube. It is interesting to compare the extracted parameters with the simulation results for the single-tube transistor described above. Considering that the measured CNTs are 10 times longer than in our simulation study which increases the capacitances roughly by a factor of ten and that the spacers are 30 times longer which increases the impact of the Schottky barriers and thereby increasing the charging resistances, the extracted parameters can be explained qualitatively with our quantum simulation study. For quantitative simulation studies, however, scattering needs to be included.

Conclusion

Self-consistent quantum simulations were developed for deriving an equivalent circuit capturing NQS effects important for circuit design and simulation. Although some problems especially regarding the contact resistance and the derivation of analytical formulas for the equivalent circuit elements are not solved yet, a comparison to measurements reveals a good correspondence between simulated and measured NQS effects.

References

[1] C. Kocabas, S. Dunham, Q. Cao, K. Cimino, X. Ho, H.-S. Kim, D. Dawson, J. Payne, M. Stuenkel, H. Zhang, T. Banks, M. Feng, S. V. Rotkin, and J. A. Rogers, "High-frequency performance of submicrometer transistors that use aligned arrays of single-walled carbon nanotubes," *Nano Letters*, vol. 9, no. 5, pp. 1937–1943, May 2009.

[2] A. L. Louarn, F. Kapche, J.-M. Bethoux, H. Happy, G. Dambrine, V. Derycke, P. Chenevier, N. Izard, M. F. Goffman, and J.-P. Bourgoin, "Intrinsic current gain cutoff frequency of 30 ghz with carbon nanotube transistors," *Applied Physics Letters*, vol. 90, no. 23, p. 233108, 2007.

[3] K. Narita, H. Hongo, M. Ishida, and F. Nihey, "High-frequency performance of multiple-channel carbon nanotube transistors," *physica status solidi (a)*, vol. 204, no. 6, pp. 1808–1813, 2007.

[4] N. Paydavosi, K. Holland, M. Zargham, and M. Vaidyanathan, "Understanding the frequency- and time-dependent behavior of ballistic carbon-nanotube transistors," *IEEE Trans. Nanotechnology*, vol. 8, no. 2, pp. 234–244, March 2009.

[5] Y. Chen, Y. Ouyang, J. Guo, and T. X. Wu, "Time-dependent quantum transport and nonquasistatic effects in carbon nanotube transistors," *Applied Physics Letters*, vol. 89, no. 20, p. 203122, 2006.

[6] D. L. John, L. C. Castro, P. Pereira, and D. L. Pulfrey, "A schrödinger-poisson solver for model carbon nanotube fets," *Proc. NSTI Nanotechnology*, vol. 3, pp. 65–68, 2004.

[7] M. Claus, S. Mothes, and M. Schröter, "A numerical device simulator for nanoscale carbon nanotube transistors," in *Semiconductor Conference Dresden*, vol. A3-3, 2009.

[8] A. Arnold, "Mathematical concepts of open quantum boundary conditions," *Transport Theory and Statistical Physics*, vol. 30, pp. 561 – 584, 2001.

[9] A. Javey, J. Guo, D. Farmer, Q. Wang, E. Yenilmez, R. Gordon, M. Lundstrom, and H. Dai, "Self-aligned ballistic molecular transistors and electrically parallel nanotube arrays," *Nano Letters*, vol. 4, pp. 1319–1322, Jun. 2004.

[10] S. Laux, "Techniques for small-signal analysis of semiconductor devices," *IEEE Trans. Computer-Aided Design of Integrated Circuits and Systems*, vol. 4, no. 4, pp. 472–481, October 1985.

[11] M. Bagheri and Y. Tsividis, "A small signal dc-to-high-frequency nonquasistatic model for the four-terminal mosfet valid in all regions of operation," *IEEE Trans. Electron Devices*, vol. 32, no. 11, pp. 2383 – 2391, nov 1985.

[12] Y. Tsividis, *Operation and Modeling of the MOS Transistor*. McGraw-Hill, 1999.

[13] R. Singh, A. Juge, R. Joly, and G. Mortin, "An investigation into the nonquasistatic effects in mos devices with on-wafer s-parameter techniques," in *IEEE Int. Conf. on Microelectronic Test Structrures*, vol. 6, mar 1993, pp. 21 –25.

[14] P. J. Burke, "Ac performance of nanoelectronics: towards a ballistic thz nanotube transistor," *Solid-State Electronics*, vol. 48, pp. 1981 – 1986, 2004.

[15] S. Salahuddin, M. Lundstrom, and S. Datta, "Transport effects on signal propagation in quantum wires," *IEEE Trans. Electron Devices*, vol. 52, no. 8, pp. 1734–1742, Aug. 2005.

[16] M. Claus and M. Schröter, "Design study of cnt transistor layouts for analog circuits," in *Proc. NSTI Workshop on Compact Modeling*, vol. 3, 2009, pp. 566 – 569.